Site-1 protease inhibits mitochondrial respiration by controlling the TGF-β target gene *Mss51*

Muhammad G. Mousa[1,5], **Lahari Vuppaladhadiam**[1,5], **Meredith O. Kelly**[1], **Terri Pietka**[1], **Shelby Ek**[1], **Karen C. Shen**[2], **Gretchen A. Meyer**[2,3,4], **Brian N. Finck**[1], **Rita T. Brookheart**[1,6,*]

[1]John T. Milliken Department of Medicine, Division of Geriatrics and Nutritional Sciences, Washington University School of Medicine, St. Louis, MO 61110, USA

[2]Program in Physical Therapy, Washington University School of Medicine, St. Louis, MO 63110, USA

[3]Departments of Orthopaedic Surgery and Neurology, Washington University School of Medicine, St. Louis, MO 63110, USA

[4]Department of Biomedical Engineering, Washington University, St. Louis, MO 63130, USA

[5]These authors contributed equally

[6]Lead contact

SUMMARY

The mitochondrial response to changes in cellular energy demand is necessary for cellular adaptation and organ function. Many genes are essential in orchestrating this response, including the transforming growth factor (TGF)-β1 target gene *Mss51*, an inhibitor of skeletal muscle mitochondrial respiration. Although Mss51 is implicated in the pathophysiology of obesity and musculoskeletal disease, how Mss51 is regulated is not entirely understood. Site-1 protease (S1P) is a key activator of several transcription factors required for cellular adaptation. However, the role of S1P in muscle is unknown. Here, we identify S1P as a negative regulator of muscle mass and mitochondrial respiration. S1P disruption in mouse skeletal muscle reduces Mss51 expression and increases muscle mass and mitochondrial respiration. The effects of S1P deficiency on mitochondrial activity are counteracted by overexpressing Mss51, suggesting that one way S1P inhibits respiration is by regulating Mss51. These discoveries expand our understanding of TGF-β signaling and S1P function.

Graphical abstract

Disrupted Site-1 Protease Function in Skeletal Muscle Impacts

Mitochondrial Metabolism

Loss of S1P

Decreased Mss51 expression

Increased respiration

Organ Size Regulation

Loss of S1P

Increased muscle mass

In brief

Mousa et al. show that site-1 protease (S1P) negatively regulates skeletal muscle mass and mitochondrial respiration. S1P inhibits respiration via its positive regulation of Mss51 expression. S1P depletion partially impairs TGF-β1-dependent Mss51 expression, implicating S1P in TGF-β1 signaling. These findings expand our understanding of the multi-faceted control of mitochondrial metabolism.

INTRODUCTION

Mitochondria are essential for the cellular response to physiologic and pathologic stimuli, such as those encountered during aging and muscular dystrophies.[1–4] These stimuli elicit dynamic changes in cellular energy demand and substrate availability that require cellular adaptation. Disrupted mitochondrial function can contribute to a failure in adaptation and is associated with several human diseases including muscular dystrophies and sarcopenia—skeletal muscle disorders that are associated with decreased muscle mass and mitochondrial function.[1–4] Studies have focused on identifying therapeutic targets to enhance mitochondrial function and thus improve adaptability in human disease states. One key example of this in skeletal muscle is the transforming growth factor (TGF)-β family of proteins that enhance muscle growth and mitochondrial metabolic capacity.[5–7] Despite advances in our understanding of the role mitochondria play in adapting to cellular

stress elicited by physiologic and pathophysiologic conditions, the molecular mechanisms by which changes in mitochondrial bioenergetics are regulated and, in the case of disease, disrupted are not yet fully understood.

Site-1 protease (S1P; also known as subtilisin/kexin-isozyme 1 or PCSK8) coordinates the adaptive response to physiologic or pathologic stimuli through its regulated intramembrane proteolysis (RIP) of key regulators important for maintaining cellular homeostasis.[8] S1P-mediated RIP is required for the proteolytic activation of several membrane-bound transcription factors, most notably the sterol regulatory element-binding proteins (SREBP) and ATF6, a key arm of the unfolded protein response.[9,10] Through RIP, S1P coordinates several important signaling pathways associated with human disease and organismal development (e.g., lipid/sterol biosynthesis, lysosomal biogenesis, and the unfolded protein response).[11–20] We previously described a patient with a *de novo,* gain-of-function mutation in S1P who exhibited altered skeletal muscle mitochondrial morphology and myoedema.[21] These findings suggested a role for S1P in skeletal muscle function and respiration. Despite the important implications of S1P in human disease and organismal development and its potential influence on skeletal muscle, few studies have directly explored the role of S1P in muscle.

Here, we show that S1P controls mitochondrial respiration and influences muscle mass. Although germline deletion of S1P is lethal, in the present study, skeletal-muscle-specific S1P knockout (S1P[smKO]) was well tolerated, and the resulting mice were viable and exhibited no obvious phenotype.[22] Interestingly, gastrocnemius muscle mass is increased in S1P[smKO] mice, and glycolytic muscle fibers from these mice have increased mitochondrial respiration. Our data suggest that one mechanism by which S1P inhibits mitochondrial respiration is by controlling the mitochondrial-localized gene *Mss51* and that this regulation partially occurs through the TGF-β1 signaling pathway. These data unveil a role for S1P in the regulation of mitochondrial respiration and identify a potential mechanism by which this occurs.

RESULTS

S1P depletion in skeletal muscle is associated with increased muscle mass

S1P function has been widely studied in liver and bone, with an emphasis on its role in cellular lipid homeostasis and proteostasis.[2,11–15] We recently described a patient with a gain-of-function mutation in S1P with a pronounced skeletal muscle phenotype, potentially implicating S1P in skeletal muscle function and respiration.[21] To determine the role of S1P (encoded by the *Mbtps1* gene) in skeletal muscle, we first examined *Mbtps1* gene expression levels in various murine muscle groups by quantitative PCR (qPCR). *Mbtps1* is expressed in mouse skeletal muscle (gastrocnemius, tibialis anterior, and soleus), with mRNA levels highest in the gastrocnemius compared with other muscle groups tested (Figure 1A). *Mbtps1* gastrocnemius mRNA levels were similar to levels in the liver, an organ widely used to study S1P function[15,22] (Figure 1A).

To investigate the role of S1P in skeletal muscle, we generated skeletal-muscle-specific S1P KO mice (S1P[smKO]) by crossing the established S1P-floxed mouse strain with mice

expressing Cre recombinase under the control of the human *ACTA1* promoter (Figure 1B).[22] Although germline deletion of S1P is embryonically lethal, homozygous S1P[smKO] mice were viable with no obvious phenotypes compared with floxed littermate controls (wild type [WT]) based on the phenotypic evaluations we performed herein.[22] Quantification of *Mbtps1* mRNA in the gastrocnemius and soleus of S1P[smKO] mice by qPCR showed a robust decrease in *Mbtps1* mRNA levels compared with WT muscles (Figure 1B).

S1P is a key regulator of SREBPs, which activate a series of target genes required for lipid and sterol biosynthesis.[23] Deletion of S1P in mouse liver inhibits SREBP activation, decreasing plasma triglyceride and cholesterol levels, underscoring the need for S1P to maintain lipid/sterol homeostasis.[22] Based on these observations, we examined whether S1P[smKO] mice had altered plasma lipid and cholesterol levels. Compared with WT littermates, S1P[smKO] mice had normal plasma lipid and cholesterol levels, as well as normal body weight and lean and fat mass (Figures S1A and S1B). We also examined activation of the SREBP pathway in S1P[smKO] by quantifying expression of SREBP target genes in skeletal muscle by qPCR and observed no differences in target gene expression between S1P[smKO] and WT muscles (Figure S1C).

To examine the impact of S1P depletion on skeletal muscle directly, we performed morphological and histological analyses of S1P[smKO] and WT muscles. At 12 weeks of age, S1P[smKO] mice exhibited a 17.6% increase in gastrocnemius mass compared with WT gastrocnemius (Figure 1C). Soleus and tibialis anterior masses and tibia length were similar between S1P[smKO] and WT mice (Figures 1C and S1D, respectively). Gastrocnemius glycogen and triglyceride content were also similar between S1P[smKO] and WT mice (Figure S1E). Gross histological examination of gastrocnemius by H&E staining indicated no overt differences in fiber organization in S1P[smKO] mice relative to WT mice (Figure 1D). We next examined fiber-type distribution and size. We observed no differences in fiber size (cross-sectional area) or the overall percentages of type I and type II fibers between KO and WT muscle (Figures 1E–1G). However, fiber-size distribution was altered in S1P[smKO] muscle, where the KO mice exhibited a greater range of fiber sizes compared with WT mice (Figure 1H). Interestingly, the total number of fibers did not vary between KO and WT muscles (Figure 1H, inset). Together these data indicate that gastrocnemius mass is increased in S1P[smKO] mice compared with WT mice but with no overt differences in fiber-type size.

Skeletal-muscle-specific depletion of S1P increased gastrocnemius muscle mass (Figure 1C) and a previous study showed that loss of S1P in bone is associated with increased muscle mass in 40-week-old mice.[24] Based on these data, we examined whether the increase in gastrocnemius muscle mass we observed in 12-week-old S1P[smKO] mice would be evident in older S1P[smKO] mice. To investigate this, we examined masses of the gastrocnemius, soleus, and tibialis anterior of 97-week-old S1P[smKO] and WT mice. Aged S1P[smKO] mice had increased mass of both the soleus and gastrocnemius compared with age-matched WT littermates (Figure 1I). Sirius red staining of gastrocnemius showed no differences in collagen expansion (i.e., fibrosis) between 97-week-old KO and WT mice (Figure S2A). Expression levels of fibrotic markers (*Col1a1*, *Col3a1*, and *Fn1*) were also unchanged

between 97-week-old S1P[smKO] and WT mice (Figure S2B). These data further suggest that depletion of S1P in skeletal muscle is associated with increased muscle mass.

S1P is a negative regulator of mitochondrial respiration

We previously described a patient with a gain-of-function mutation in S1P with altered skeletal muscle mitochondrial morphology, implicating a role for S1P in skeletal muscle mitochondrial function.[21] Moreover, a recent study showed that S1P can localize to the mitochondria of human keratinocytes and alter mitochondrial respiration.[25] To examine whether skeletal-muscle-specific depletion of S1P impacts mitochondrial respiration in muscle, we measured respiration in the gastrocnemius of S1P[smKO] and WT mice. Because S1P is highly expressed in gastrocnemius and the gastrocnemius mass of S1P[smKO] mice is greater than that of WT mice, we focused on this muscle. The gastrocnemius is composed of glycolytic (fast-twitch) and oxidative (slow-twitch) muscle fibers, which vary in their mitochondrial substrate preferences.[26] The "white" gastrocnemius, noted for its opaqueness, is primarily composed of glycolytic fibers, while the "red" gastrocnemius mainly consists of oxidative fibers. Thus, we examined the oxidative capacity of permeabilized white and red gastrocnemius fibers separately. Palmitoylcarnitine-mediated mitochondrial respiration was unaltered in both the red and white gastrocnemius fibers of S1P[smKO] mice (Figure 2A). Pyruvate-mediated respiration was unchanged in the red gastrocnemius of S1P[smKO] mice relative to WT mice (Figure 2B, left graph). In contrast, when we measured pyruvate-mediated mitochondrial respiration in the primarily glycolytic fibers of the white gastrocnemius, complex I + complex II respiration and electron transport chain capacity were higher in the white gastrocnemius of S1P[smKO] mice relative to WT mice (Figure 2B, right graph). These findings indicate S1P is a negative regulator of pyruvate-mediated respiration in gastrocnemius glycolytic muscle fibers.

To further characterize the mitochondria of S1P[smKO] skeletal muscle, we measured mitochondrial DNA content and expression levels of *Pgc-1α* and *Tfam* in S1P[smKO] and WT gastrocnemius, markers of mitochondrial number and biogenesis.[27] Depletion of S1P from skeletal muscle did not alter mitochondrial DNA content (Figure 2C), and transcript levels of *Pgc-1α* and *Tfam* were unchanged between S1P[smKO] and WT gastrocnemius (Figure 2D). To determine whether changes in mitochondrial respiration were a result of altered expression of mitochondrial electron transport chain (ETC) complexes, we measured ETC protein levels by western blot and detected no differences in ETC complex protein levels (Figure 2E). These data suggest that the increase in muscle mitochondrial respiration was not due to increased mitochondrial abundance or altered ETC expression levels.

S1P inhibits mitochondrial respiration by promoting Mss51 expression

To identify the mechanism by which S1P controls mitochondrial respiration, we performed RNA sequencing (RNA-seq) on RNA isolated from the gastrocnemius of 12-week-old S1P[smKO] and WT littermates (n = 4 per genotype). We identified 75 significantly differentially expressed genes (60 up-regulated and 15 down-regulated) with fold change values greater than 1.5 and p values less than 0.05 in the gastrocnemius of S1P[smKO] mice relative to WT mice (Figure 3A; Table S2).

One candidate gene that caught our interest was *Mss51*, as the expression of *Mss51* was dramatically decreased in the gastrocnemius of S1P[smKO] mice compared with WT mice (Figure 3A). To validate our *Mss51* RNA-seq results, we measured *Mss51* mRNA levels by qPCR in the gastrocnemius of S1P[smKO] and WT mice. Our analysis showed decreased expression of *Mss51* transcript levels in the gastrocnemius of S1P[smKO] mice compared with WT mice, confirming our RNA-seq results (Figure 3B). Mss51 is primarily expressed in glycolytic muscle fibers, where it negatively regulates mitochondrial respiration, but is not involved in mitochondrial biogenesis.[6,7,28,29] Indeed, our soleus RNA-seq data (Table S3) and subsequent qPCR analysis of *Mss51* expression in the soleus (a primarily oxidative muscle) showed there was no change in *Mss51* transcript levels in the soleus of S1P[smKO] mice relative to WT mice (Figure 3C). These reported characteristics of Mss51 mirror our observations of muscle group-specific effects of S1P deficiency.

To further validate our findings that depletion of S1P decreases *Mss51* expression, we transiently knocked down *Mbtps1* in the murine C2C12 cell line using small interfering RNA (siRNA) oligos to target *Mbtps1* (Figure 3D) and measured *Mss51* transcript levels by qPCR. C2C12 cells transfected with scrambled siRNA served as a negative control. Relative to negative control siRNA cells, depletion of S1P in C2C12 cells decreased *Mss51* expression, recapitulating both our RNA-seq and *in vivo* qPCR results (Figure 3E). These data indicate that S1P is a positive regulator of Mss51 expression.

Because S1P is required for differentiation in other cell types and our studies use differentiated C2C12 cells, we examined whether S1P depletion blocked the ability of C2C12 cells to differentiate as an additional control to our cell culture studies.[1] S1P siRNA knockdown cells readily differentiated into myotubes, as examined by staining for myosin heavy chain—a myotube marker (Figure S2D).[30]

Because S1P is a positive regulator of Mss51 expression and Mss51 inhibits mitochondrial respiration, we hypothesized that restoring Mss51 expression in S1P-depleted cells would decrease mitochondrial respiration.[6,7] To test our hypothesis, we used Seahorse respirometry to quantify oxidative respiration in S1P siRNA knockdown and negative control siRNA (control) cells that overexpress either empty vector or FLAG-tagged Mss51. S1P siRNA knockdown cells had increased rates of basal and maximal respiration compared with control cells (Figures 3F and 3G). There was also a potential trend for increased ATP production and spare respiratory capacity in S1P siRNA knockdown cells relative to control cells. Strikingly, S1P siRNA knockdown cells expressing Mss51 had decreased respiratory parameters (decreased basal and maximal respiration and spare respiratory capacity) and a trend for decreased ATP production compared with S1P siRNA knockdown cells expressing empty vector (Figures 3F and 3G). The Mss51-driven decline in mitochondrial respiration has been previously reported in C2C12 cells, thus we sought to recapitulate these findings by depleting *Mss51* with siRNAs in C2C12 cells and measuring mitochondrial respiration. Indeed, knockdown of *Mss51* resulted in increased basal respiration and ATP production (Figures S4C and S4D). Together, these data suggest that one mechanism by which S1P inhibits mitochondrial respiration is through Mss51.

S1P is involved in the induction of Mss51 expression by TGF-β1

TGF-β1 and its family of ligands induce Mss51 expression through an as-yet unknown mechanism. To determine if the induction of Mss51 by TGF-β1 requires S1P, we treated S1P knockdown and negative control siRNA (control) C2C12 cells with either vehicle or recombinant TGF-β1 and measured *Mss51* expression by qPCR. In the presence of TGF-β1, *Mss51* expression was increased in both control and S1P-depleted cells; however, the TGF-β1-mediated induction of *Mss51* expression was significantly attenuated in S1P-depleted cells compared with control-treated cells (Figure 4A). These data demonstrate that S1P positively regulates *Mss51* expression by TGF-β1.

To date, S1P has not been shown to modulate TGF-β1 signaling. TGF-β1 can regulate cellular function through both Smad-dependent and Smad-independent signaling pathways.[31] To examine the function of S1P on TGF-β1 signaling and gain insight into the mechanism of S1P-driven Mss51 expression, we first investigated TGF-β1-induced Smad activation. Binding of TGF-β1 to its receptors triggers the phosphorylation and activation of the transcription factor Smad 2, thus Smad 2 phosphorylation is a positive marker of TGF-β1 Smad-dependent signaling.[32] We assessed the phosphorylation status of Smad 2 in whole-cell lysates from vehicle (untreated) and TGF-β1-treated control and S1P-depleted cells by western blot. Smad 2 phosphorylation was not detectable in untreated cells, but Smad 2 phosphorylation was equally induced in control and S1P-depleted cells treated with TGF-β1 (Figure 4B). These data suggest S1P controls TGF-β1-induced Mss51 expression independently of Smad 2 phosphorylation/activation.

We next examined TGF-β1 Smad-independent signaling, which includes TGF-β1-driven Akt activation through phosphorylation of Akt on Ser473.[31] We assessed levels of phosphorylated Akt^{Ser473} and total Akt in untreated and TGF-β1-treated control and S1P-depleted cells. S1P-depleted cells treated with TGF-β1 had similar levels of phosphorylated Akt compared with treated control cells (Figure 4C), suggesting that S1P depletion does not alter TGF-β1-dependent activation of Akt.

DISCUSSION

In the present study, we investigated the biological role of S1P in skeletal muscle using a skeletal-muscle-specific S1P KO mouse line and identified S1P as a regulator of skeletal muscle mass and mitochondrial respiration. Specifically, S1P^{smKO} mice have increased gastrocnemius muscle mass, and, as mice age, this increase in mass is present in both gastrocnemius and soleus muscles relative to age-matched control littermates. How S1P regulates this change in muscle mass is not clear. Further studies are underway to explore the connection between S1P expression and muscle mass. With regards to controlling mitochondrial respiration, we show that S1P^{smKO} mouse gastrocnemius and S1P siRNA knockdown C2C12 cells have increased mitochondrial respiration. Exogenous expression of Mss51 obliterated the increase in respiration observed in S1P siRNA knockdown cells, indicating that one mechanism by which S1P inhibits mitochondrial respiration is by driving Mss51 expression.

Our S1P^{smKO} studies show increased pyruvate-mediated mitochondrial respiration in predominately glycolytic muscle fibers but not in oxidative fibers of the gastrocnemius. This may be due to increased abundance or activity of S1P in glycolytic fibers relative to oxidative fibers, as has been reported for the S1P substrate SREBP-1c.[33] Moreover, Mss51 abundance is predominantly concentrated in glycolytic muscle relative to oxidative muscle, with a lower degree of expression in other tissues (e.g., heart, liver, and adipose).[6,7,28,29] Indeed, our RNA-seq and qPCR analysis of the primarily oxidative mouse soleus showed no change in *Mss51* transcript levels between S1P^{smKO} and WT solei, thus suggesting S1P-dependent control of mitochondrial respiration is focused on glycolytic fibers in the gastrocnemius and that S1P may have an as-yet unknown function in oxidative muscles.

Palmitoylcarnitine-mediated respiration was unaltered in the gastrocnemius of S1P^{smKO} mice, suggesting that S1P may not control long-chain fatty acid substrate-mediated respiration. Our data are specific for long-chain fatty acids since palmitoylcarnitine requires carnitine palmitoyltransferase 2 (CPT2) to pass through the inner mitochondrial membrane. It is possible that medium-chain fatty acids, which do not require CPT2, may illicit a different response.

Chen et al. recently reported that S1P knockdown in a human keratinocyte cell line decreased mitochondrial respiration and is in opposition to what we report here.[25] One key reason for this discrepancy is that both studies used different cell types originating from different organisms (e.g., human keratinocytes versus isolated murine fibers and cultured murine myotubes).

Our depletion of Mss51 alone increased basal respiration and ATP production in C2C12 cells—recapitulating the results of Moyer et al.[7] We show that S1P depletion increased mitochondrial respiration with a trending increase in ATP production and that these increases are inhibited by the addition of Mss51. These data suggest that one mechanism by which S1P inhibits mitochondrial respiration is via control of Mss51. In contrast, when we expressed Myc-FLAG-tagged S1P in C2C12 cells, *Mss51* mRNA expression was unaltered, and no significant changes in respiration were observed (Figures S4E–S4I). Failure to see an increase in *Mss51* expression suggests that overexpression of S1P alone is not sufficient to alter *Mss51* transcript levels. Moreover, it is possible that the epitope tags on our S1P plasmid may negatively impact the ability of S1P to function in the context of Mss51 regulation and respiration. Current studies are underway to define the mechanisms by which S1P regulates Mss51 expression and mitochondrial respiration.

We show that Mss51 expression is decreased by S1P depletion in both mouse gastrocnemius and cultured myotubes. In mammals, little is known about the factors that control Mss51 expression, and even less is understood about how Mss51 modulates mitochondrial respiration. It is known that members of the TGF-β1 family of ligands induce Mss51 expression via an as-yet unknown mechanism. Here, we begin to explore how S1P controls Mss51 expression and show that siRNA depletion of S1P in cultured myotubes partially inhibits TGF-β1-driven *Mss51* expression. One drawback to our siRNA system is that S1P was depleted, not completely knocked down, and thus it is possible the remaining amounts of S1P enzyme were sufficient to drive blunted, yet detectable, levels of Mss51 expression.

Because depletion of S1P impacted TGF-β1-dependent Mss51 expression, this suggested a role for S1P in controlling TGF-β1 signaling pathways. To begin to explore this possibility, we examined whether S1P modulated TGF-β1 signaling via Smad-dependent or Smad-independent signaling pathways and demonstrated that depletion of S1P did not impact Smad 2 phosphorylation nor Akt phosphorylation. Whether S1P controls Smad and Akt activity downstream of phosphorylation are not known. Analysis of our RNA-seq data of mouse gastrocnemius showed no significant changes in TGF-β1 receptors or SMAD genes; however, our analyses showed decreased expression of genes regulated by several transcription factors, one in particular being the transcription factor YY1 (Figures S3A and S3B). YY1 is a modulator of TGF-β/SMAD signaling.[34–37] To date, whether YY1 influences TGF-β/SMAD signaling in skeletal muscle is not clear and is a focus of our ongoing studies.

In conclusion, these studies identify S1P as a regulator of mitochondrial respiration. Our data also shed light on the regulation of Mss51 by linking S1P to TGF-β1 signaling. Together, our findings uncover a function for S1P in mitochondrial biology and implicate S1P in the adaptation to disruptions in skeletal muscle respiration. Current work is focused on examining the mechanism(s) by which S1P modulates mitochondrial function and the implications this may have on human disease states.

Limitations of the study

The experiments performed in this study indicate that S1P controls Mss51 expression, and one way by which it does so is downstream of TGF-β1 signaling. How TGF-β1 controls Mss51 expression remains unknown. Our ongoing follow-up studies aim to define the mechanism by which S1P controls Mss51 and mitochondrial respiration. Future studies should include examination of other TGF-β1 signaling arms beyond the Smad 2 and Akt targets explored in this study (e.g., Smad 3, nuclear factor κB [NF-κB], and mitogen-activated protein kinase [MAPK]), to define how S1P functions in TGF-β1 signaling. Furthermore, to link TGF-β1 signaling directly to S1P-Mss51-regulated mitochondrial respiration, future studies should examine respiration in S1P siRNA and Mss51 siRNA knockdown cells in the absence and presence of TGF-β1.

STAR★METHODS

RESOURCE AVAILABILITY

Lead contact—Further information and requests for resources and reagents should be directed to and will be fulfilled by the lead contact, Rita T. Brookheart rbrookheart@wustl.edu.

Materials availability—Mouse lines generated in this study are available upon request to the lead contact.

Data and code availability—RNA-Seq data have been deposited at NCBI GEO and are publicly available as of the date of publication. The accession number is listed in the key

resources table. Original Western blot images and microscopy data reported in this paper will be shared by the lead contact upon request.

This paper does not report original code.

Any additional information required to reanalyze the data reported in this paper is available from the lead contact upon request.

EXPERIMENTAL MODEL AND SUBJECT DETAILS

Mice—S1P floxed mice in the C57BL/6J background were previously described[22] and obtained from Linda Sandell at Washington University, with generous permission from Jay Horton of University of Texas Southwestern. HSA-Cre79 (B6.Cg-Tg(ACTA1-cre)79Jme/J; Stock No. 006149) mice were obtained from Jackson Laboratory in the C57BL/6J background. S1P floxed mice were crossed with HSA-Cre79 mice to generate skeletal-muscle-specific S1P knockout mice. Littermates not expressing Cre recombinase were used as controls for all experiments. Mice were genotyped for the presence of Cre recombinase and floxed S1P allele using gene-specific primers.[22] Primer sequences are listed in Table S1. Studies were performed using male mice aged 12 and 97 weeks (specific mouse ages are indicated in the figure legends). Mice were maintained on a standard laboratory chow diet and group housed on a 12 h light/dark cycle.

Cell lines—All cells were grown at 37°C with 5% CO^2. C2C12 cells (ATCC) were grown in DMEM supplemented with 10% fetal bovine serum and 1% Penicillin-Streptomycin. To differentiate C2C12 myoblasts into myotubes, cells were grown to 80% confluency, washed with 1x PBS and grown in DMEM supplemented with 2% horse serum for 2–3 days as indicated in the methods below.

Study approval—All mouse studies were approved by the Institutional Animal Care and Use Committee of Washington University.

METHOD DETAILS

Body composition—ECHO MRI was used to measure body composition in unanesthetized mice using an ECHOMRI 3-1 (ECHO Medical Systems).

Serum and muscle metabolites—For serum metabolite analyses, chow-fed mice were fasted for 4 h (09:00–13:00h) followed by tail-vein blood withdrawal. Blood was collected by venipuncture of the inferior vena cava and processed for plasma collection via centrifugation in EDTA-coated tubes, and frozen in liquid nitrogen. Plasma triglyceride and cholesterol levels were measured enzymatically via the Infinity triglyceride (TR22421) and cholesterol (TR13421) assay kits (Thermo Fisher) as per manufacturer's instructions. Gastrocnemius muscle was harvested and immediately snap frozen in liquid nitrogen. Gastrocnemius glycogen content was measured using the Sigma Glucose Oxidase Assay Kit (GAGO-20) as reported previously.[39] Gastrocnemius triglyceride levels were measured by homogenizing muscles in chloroform-methanol (2:1 *v/v*), centrifuged to collect the organic phase, dried, resuspended in Triglycerides Reagents (TR22421, Thermo Fisher Scientific), and triglyceride levels measured by absorbance as per manufacturer's instructions.

Histological analyses—Tragacanth gum was placed on top of corks and fresh muscles were vertically placed in the gum so that ¼ of the muscle was embedded. Samples were submerged in cold (−150°C) isopentane as described[40] for 20 s, and immediately stored at −80°C until sectioning. Frozen muscles were transversely cryosectioned into 10 μM thick sections at the mid-belly on a cryostat (Leica Biosystems). Sections were stained with haematoxylin (H&E), Sirius Red, DAPI, or immunostained against myosin heavy chain isoforms (type I (BA-F8), type IIa (SC-71), type IIx (no staining indicated IIx fibers), and type IIb (BF-F3); Developmental Studies Hybridoma Bank) and laminin (ab11575, Abcam). Cross sectional area, fiber size, and fiber type distribution of each fiber type was quantified from immunostained fiber type images in ImageJ as reported previously.[38,41]

Gene expression analysis—Total RNA was isolated from C2C12 cells, skeletal muscle, heart, adipose, kidney, and liver with RNA STAT-60 (Tel-Test Inc) as per manufacturer's instructions. For tissues, RNA was isolated by disrupting tissue in RNA STAT-60 using 5 mm steel beads (Qiagen) and a TissueLyser II (Qiagen). RNA was reverse transcribed into cDNA using the High-Capacity cDNA Reverse Transcription Kit (Applied Biosystems). Quantitative real-time PCR was performed using Power SYBR green (Applied Biosystems) and transcripts quantified on an ABI QuantiStudio 3 sequence detection system (Applied Biosystems). Data was normalized to 36B4 expression, unless otherwise noted, and results analyzed using the $2^{-\Delta\Delta Ct}$ method and reported as relative units to controls. Primer sequences are listed in Table S1.

RNA-seq analysis—Whole gastrocnemius and soleus were harvested from 12-week-old male floxed (wild-type) and S1P-skeletal muscle-specific knockout mice and immediately snap frozen in liquid nitrogen for a total of n = 4 mice per genotype examined. RNA was isolated from tissue as described above. RNA was DNase I treated as per manufacturer's instructions (RNase-Free DNase Set, Qiagen) then cleaned up and eluted with RNAse and DNAse free molecular grade water (RNeasy MinElute Cleanup Kit, Qiagen), followed by quantification (NanoDrop, Thermo Fisher Scientific). RNA with RIN values greater than 8 were accepted for RNASeq. Samples were prepared according to library kit manufacturer's protocol, indexed, pooled, and sequenced on an Illumina HiSeq. Basecalls and demultiplexing were performed with Illumina's bcl2fastq software and a custom python demultiplexing program with a maximum of one mismatch in the indexing read. RNA-seq reads were aligned to the Ensembl release 76 primary assembly with STAR version 2.5.1a.[42] Gene counts were derived from the number of uniquely aligned unambiguous reads by Subread:featureCount version 1.4.6-p5.[43] Isoform expression of known Ensembl transcripts were estimated with Salmon version 0.8.2.[44] Sequencing performance was assessed for the total number of aligned reads, total number of uniquely aligned reads, and features detected. The ribosomal fraction, known junction saturation, and read distribution over known gene models were quantified with RSeQC version 2.6.2.[45]

All gene counts were then imported into the R/Bioconductor package EdgeR[46] and TMM normalization size factors were calculated to adjust samples for differences in library size. Ribosomal genes and genes not expressed in the smallest group size minus one sample greater than one count-per-million were excluded from further analysis. The TMM size

factors and the matrix of counts were then imported into the R/Bioconductor package Limma.[47] Weighted likelihood based on the observed mean-variance relationship of every gene and sample were then calculated for all samples with the voomWithQualityWeights.[48] The performance of all genes was assessed with plots of the residual standard deviation of every gene to their average log-count with a robustly fitted trend line of the residuals. Differential expression analysis was then performed to analyze differences between conditions and the results were filtered for only those genes with Benjamini-Hochberg false-discovery rate adjusted p values less than or equal to 0.05.

The accession number for the RNA-seq data reported in this study is deposited at NCBI GEO under accession number GSE199014 located at https://www.ncbi.nlm.nih.gov/geo/query/acc.cgi?acc=GSE199014.

siRNA studies and TGF-β1 treatment—C2C12 cells were plated onto 6-well plates at a 2×10^5 density and 24 h later transfected with either negative control siRNA (Negative Control No.1 siRNA, Life Technologies) or custom siRNAs targeting *Mbtps1* or *Mss51* (Silencer Select siRNAs, Life Technologies) using Lipofectamine RNAiMAX as per manufacturer's instructions. After 48 h, cells were differentiated with DMEM supplemented with 2% horse serum. Two days after differentiation, cells were harvested for gene expression analysis. For TGF-β1 treatment studies, three days post-differentiation, cells were treated with 50 ng/mL TGF-β1 (R&D) for 5 h then harvested for downstream endpoints. For myosin heavy chain (MHC) staining, cells were differentiated for 2 days then fixed in paraformaldehyde and stained for MHC (MF-20; Developmental Studies Hybridoma Bank) and DAPI prior to imaging.

Seahorse OCR analysis—Cellular respiration was measured on a Seahorse XFe24 Analyzer (Agilent). C2C12 cells were plated onto 24-well Seahorse XF24 cell culture microplates at a 8,000 cell density and 24 h later co-transfected with either negative control siRNA (Negative Control No.1 siRNA, Life Technologies) with empty vector (pCMV6-Entry; Origene PS100001) or a custom siRNA targeting *Mbtps1* (Silencer Select siRNAs, Life Technologies) with empty vector (pCMV6-Entry; Origene PS100001) or mouse Mss51-Myc-FLAG (mouse cDNA clone; Origene MR217897) using Lipofectamine 2000 (Life Technologies) as per manufacturer's instructions. For Mss51 studies, cells were treated as above, but instead were transfected with negative control siRNA (Negative Control No.1 siRNA, Life Technologies) or custom siRNA targeting *Mss51* using RNAiMAX (Life Technologies) as per manufacturer's instructions. For S1P overexpression studies, cells were treated as above, but transfected with empty vector (pCMV6-Entry; Origene PS100001) or mouse S1P-Myc-FLAG (mouse cDNA clone; Origene RC212265) using Lipofectamine 2000 (Life Technologies) as per manufacturer's instructions. After 48 h, cells were washed with 1x PBS and switched to differentiation media (DMEM and 2% horse serum) for 2–3 days. Cells were fed Seahorse XF-DMEM with 1 mM pyruvate, 10 mM glucose, and 2 mM glutamine and incubated in a CO^2-free incubator at 37°C for 1 h. Basal oxygen consumption rates were measured first followed by OCR measurements upon sequential addition of oligomycin (1 μM), carbonyl cyanide p-trifluoro-methoxyphenyl hydrazone (FCCP; 1 μM), and rotenone and actinomycin A (0.5 μM each) as per the Seahorse Mitochondrial Stress

Test protocol. After completion of the assay, whole protein lysates for each well were quantified by BCA assay and total protein amounts were used for normalization of Seahorse data using Wave Software (Agilent). Basal OCR, maximal respiration, protein leakage, and spare respirometry capacity were calculated using the Seahorse XF Cell Mito Stress Test Report Generator via Wave Software (Agilent) normalized to total protein levels.

Preparation of permeabilized muscle fibers and high-resolution respirometry
—Freshly isolated red and white gastrocnemius sections were immersed in cold BIOPS (10 mM EGTA, 50 mM MES, 0.5 mM DTT, 6.56 mM MgCL2, 5.77 mM ATP, 20 mM Imidazole and 15 mM phosphocreatine, pH 7.1). Tissue was trimmed of surrounding fat tissue and fibers mechanically separated on ice. Separated fibers were permeabilized with BIOPS solution containing 50 μg/mL saponin for 20 min at 4°C. Following permeabilization, fibers were washed for 15 min in ice-cold mitochondrial respiration solution (MIR05, 0.5 mM EGTA, 3 mM MgCl2, 60 mM K-lactobionate, 20 mM taurin, 10 mM KH2PO4, 20 mM HEPES, 110 mM sucrose and 1 g/L BSA, pH 7.1). Fibers were then blotted dry, weighed (3–5 mg total tissue weight) and placed in a Oxygraph-2K (OROBOROS Instruments) chamber containing 2 mL of 37°C MirO5 (supplemented with 10 μM blebbistatin and 20 mM creatine). Routine oxygen consumption was measured by the sequential addition of the following substrates: malate (0.5 mM), glutamate (10 mM) and pyruvate (5 mM) to assess complex I mediated LEAK respiration. Adenosine diphosphate (ADP, 5 mM) to assess maximal complex I maximal respiration followed by succinate (10 mM) to measure OXPHOS (complex I and II mediated respiration). The uncoupling agent FCCP (carbonyl cyanide p-trifluoro-methoxyphenyl hydrazone, 0.5 μM, titrated 3X) was then added to determine maximal electron transport system (ETS) capacity. Proper fiber preparation was determined by assessing the intactness of the outer mitochondrial membrane by adding cytochrome *c* (10 μM) after the addition of ADP. Fibers with a cytochrome c-stimulated respiration rate greater than 15% of the ADP-only rate were considered damaged and not used in our studies.[49] A period of stabilization followed the addition of each substrate and the oxygen flux per mass was recorded using the DatLab Software (OROBOROS Instruments).

Mitochondrial content—DNA was isolated from 25 mg of either whole or white gastrocnemius of S1P^{smKO} and WT mice using the DNeasy Blood & Tissue Kit (Qiagen) following manufacturer's instructions. DNA concentrations were measured via NanoDrop (Thermo Scientific) and 10 ng of DNA was used for qPCR analysis using primers specific to a mitochondrial encoded gene DNA (Cox2) and nuclear encoded gene (36B4) and Power SYBR Green (Applied Biosystems). Transcripts were quantified on an ABI QuantiStudio 3 sequence detection system (Applied Biosystems) and Cox2 expression was normalized to 36B4 expression, and results analyzed using the $2^{-\Delta\Delta Ct}$ method and reported as relative units to controls. Primer sequences are listed in Table S1.

Western blotting—Skeletal muscle whole protein lysates were generated by homogenizing tissues in lysis buffer (20 mM Tris, 15 mM NaCl, 1 mM EDTA, 0.2% NP-40, and 10% glycerol) supplemented with 2x Protease Complete cocktail tablet (Roche) and 1x Phosphatase Inhibitors (Roche, Mannheim, Germany) with stainless steel beads in

a TissueLyzer II (Qiagen). Protein lysates were rotated for 45 min at 4°C, followed by centrifugation at $15,000 \times g$ for 15 min at 4°C. Protein was quantified by bicinchoninic acid assay (BCA, Pierce Biotechnology), equal amounts of protein were resolved on a 4–15% SDS-PAGE gradient gel (Bio-Rad), and transferred to PVDF-FL membrane (MilliporeSigma). Blots were probed with appropriate primary and secondary antibodies and proteins visualized by LI-COR Odyssey imaging system. To visualize phosphorylated Smad 2, blots were incubated with SignalFire ECL Reagent (Cell Signaling) and protein visualized with a BioRad ChemiDoc XRS+. The following antibodies were used in our studies at a 1:1000 dilution: alpha tubulin (T5168, Sigma); S1P (RP-3, Triple Point Biologics Inc.); OXPHOS (MS604–300, Abcam); Phospho-Smad2 (Ser465/467) (3108, Cell Signaling); Smad 2 (5339, Cell Signaling); Phospho-Akt (4060, Cell Signaling), and Total-Akt (2920, Cell Signaling). Densitometry analysis was performed using LI-COR Image Studio Lite.

QUANTIFICATION AND STATISTICAL ANALYSIS

Normality of data distributions was assessed with graphical inspection and the Shapiro-Wilk test. For data that are normally distributed, two groups were compared using an unpaired t test and the Satterthwaite adjustment was applied when the homogeneity of variance assumption was violated. For data that are not normally distributed, groups were compared using a Wilcoxon two-sample test. Since it is known that estimation of data dispersion with small samples is inadequate, analyses with groups containing three observations were always analyzed with the Wilcoxon test.[50] Analyses were performed with SAS software, version 9.4 of the SAS System for Windows (SAS Institute Inc., Cary, NC, USA). A p value <0.05 was considered statistically significant. Data are reported as ± SEM. Statistical details and the number of samples used in each study are indicated in the figure legends and figures.

Supplementary Material

Refer to Web version on PubMed Central for supplementary material.

ACKNOWLEDGMENTS

INCLUSION AND DIVERSITY

One or more of the authors of this paper self-identifies as an underrepresented ethnic minority in their field of research or within their geographical location. While citing references scientifically relevant for this work, we also actively worked to promote gender balance in our reference list.

REFERENCES

1. Moore TM, Lin AJ, Strumwasser AR, Cory K, Whitney K, Ho T, Ho T, Lee JL, Rucker DH, Nguyen CQ, et al. (2020). Mitochondrial dysfunction is an early consequence of partial or Complete dystrophin loss in mdx mice. Front. Physiol 11, 690. 10.3389/FPHYS.2020.00690. [PubMed: 32636760]

2. Hughes MC, Ramos SV, Turnbull PC, Rebalka IA, Cao A, Monaco CMF, Varah NE, Edgett BA, Huber JS, Tadi P, et al. (2019). Early myopathy in Duchenne muscular dystrophy is associated with elevated mitochondrial H2O2 emission during impaired oxidative phosphorylation. J. Cachexia Sarcopenia Muscle 10, 643–661. 10.1002/JCSM.12405. [PubMed: 30938481]

3. Tezze C, Romanello V, Desbats MA, Fadini GP, Albiero M, Favaro G, Ciciliot S, Soriano ME, Morbidoni V, Cerqua C, et al. (2017). Age-associated loss of OPA1 in muscle impacts muscle mass, metabolic homeostasis, systemic inflammation, and epithelial senescence. Cell Metab. 25, 1374–1389.e6. 10.1016/J.CMET.2017.04.021. [PubMed: 28552492]

4. Ibebunjo C, Chick JM, Kendall T, Eash JK, Li C, Zhang Y, Vickers C, Wu Z, Clarke BA, Shi J, et al. (2013). Genomic and proteomic profiling reveals reduced mitochondrial function and disruption of the neuromuscular junction driving rat sarcopenia. Mol. Cell Biol 33, 194–212. 10.1128/MCB.01036-12. [PubMed: 23109432]

5. McPherron AC, Lawler AM, and Lee SJ (1997). Regulation of skeletal muscle mass in mice by a new TGF-beta superfamily member. Nature 387, 83–90. 10.1038/387083A0. [PubMed: 9139826]

6. Rovira Gonzalez YI, Moyer AL, LeTexier NJ, Bratti AD, Feng S, Sun C, Liu T, Mula J, Jha P, Iyer SR, et al. (2019). Mss51 deletion enhances muscle metabolism and glucose homeostasis in mice. JCI Insight 4, e122247. 10.1172/JCI.INSIGHT.122247. [PubMed: 31527314]

7. Moyer AL, and Wagner KR (2015). Mammalian Mss51 is a skeletal muscle-specific gene modulating cellular metabolism. J. Neuromuscul. Dis 2, 371–385. 10.3233/JND-150119. [PubMed: 26634192]

8. Ye J (2020). Transcription factors activated through RIP (regulated intramembrane proteolysis) and RAT (regulated alternative translocation). J. Biol. Chem 295, 10271–10280. 10.1074/JBC.REV120.012669. [PubMed: 32487748]

9. Sakai J, Rawson RB, Espenshade PJ, Cheng D, Seegmiller AC, Goldstein JL, and Brown MS (1998). Molecular identification of the sterol-regulated luminal protease that cleaves SREBPs and controls lipid composition of animal cells. Mol. Cell 2, 505–514. 10.1016/S1097-2765(00)80150-1. [PubMed: 9809072]

10. Ye J, Rawson RB, Komuro R, Chen X, Davé UP, Prywes R, Brown MS, and Goldstein JL (2000). ER stress induces cleavage of membrane-bound ATF6 by the same proteases that process SREBPs. Mol. Cell 6, 1355–1364. 10.1016/S1097-2765(00)00133-7. [PubMed: 11163209]

11. Marschner K, Kollmann K, Schweizer M, Braulke T, and Pohl S (2011). A key enzyme in the biogenesis of lysosomes is a protease that regulates cholesterol metabolism. Science 333, 87–90. 10.1126/science.1205677. [PubMed: 21719679]

12. Patra D, Xing X, Davies S, Bryan J, Franz C, Hunziker EB, and Sandell LJ (2007). Site-1 protease is essential for endochondral bone formation in mice. J. Cell Biol 179, 687–700. 10.1083/jcb.200708092. [PubMed: 18025304]

13. Patra D, DeLassus E, Liang G, and Sandell LJ (2014). Cartilage-specific ablation of site-1 protease in mice results in the endoplasmic reticulum entrapment of type IIb procollagen and down-regulation of cholesterol and lipid homeostasis. PLoS One 9, e105674. 10.1371/journal.pone.0105674. [PubMed: 25147951]

14. Patra D, DeLassus E, Hayashi S, and Sandell LJ (2011). Site-1 protease is essential to growth plate maintenance and is a critical regulator of chondrocyte hypertrophic differentiation in postnatal mice. J. Biol. Chem 286, 29227–29240. 10.1074/jbc.M110.208686. [PubMed: 21652717]

15. Kim JY, Garcia-Carbonell R, Yamachika S, Zhao P, Dhar D, Loomba R, Kaufman RJ, Saltiel AR, and Karin M (2018). ER stress drives lipogenesis and steatohepatitis via caspase-2 activation of S1P. Cell 175, 133–145.e15. 10.1016/j.cell.2018.08.020. [PubMed: 30220454]

16. Raggo C, Rapin N, Stirling J, Gobeil P, Smith-Windsor E, O'Hare P, and Misra V (2002). Luman, the cellular counterpart of herpes simplex virus VP16, is processed by regulated intramembrane proteolysis. Mol. Cell Biol 22, 5639–5649. [PubMed: 12138176]

17. Kondo Y, Fu J, Wang H, Hoover C, McDaniel JM, Steet R, Patra D, Song J, Pollard L, Cathey S, et al. (2018). Site-1 protease deficiency causes human skeletal dysplasia due to defective inter-organelle protein trafficking. JCI Insight 3, e121596. 10.1172/JCI.INSIGHT.121596. [PubMed: 30046013]

18. Brandl K, Rutschmann S, Li X, Du X, Xiao N, Schnabl B, Brenner DA, and Beutler B (2009). Enhanced sensitivity to DSS colitis caused by a hypomorphic Mbtps1 mutation disrupting the ATF6-driven unfolded protein response. Proc. Natl. Acad. Sci. USA 106, 3300–3305. 10.1073/pnas.0813036106. [PubMed: 19202076]

19. Bergeron É, Vincent MJ, and Nichol ST (2007). Crimean-Congo hemorrhagic fever virus glycoprotein processing by the endoprotease SKI-1/S1P is critical for virus infectivity. J. Virol 81, 13271–13276. 10.1128/JVI.01647-07. [PubMed: 17898072]

20. Olmstead AD, Knecht W, Lazarov I, Dixit SB, and Jean F (2012). Human subtilase SKI-1/S1P is a master regulator of the HCV lifecycle and a potential host cell target for developing indirect-acting antiviral agents. PLoS Pathog. 8, e1002468. 10.1371/journal.ppat.1002468. [PubMed: 22241994]

21. Schweitzer GG, Gan C, Bucelli RC, Wegner D, Schmidt RE, Shinawi M, Finck BN, and Brookheart RT (2019). A mutation in Site-1 Protease is associated with a complex phenotype that includes episodic hyperCKemia and focal myoedema. Mol. Genet. Genomic Med 7, e00733. 10.1002/mgg3.733. [PubMed: 31070020]

22. Yang J, Goldstein JL, Hammer RE, Moon YA, Brown MS, and Horton JD (2001). Decreased lipid synthesis in livers of mice with disrupted Site-1 protease gene. Proc. Natl. Acad. Sci. USA 98, 13607–13612. 10.1073/pnas.201524598. [PubMed: 11717426]

23. Espenshade PJ, and Hughes AL (2007). Regulation of sterol synthesis in eukaryotes. Annu. Rev. Genet 41, 401–427. 10.1146/annurev.genet.41.110306.130315. [PubMed: 17666007]

24. Gorski JP, Huffman NT, Vallejo J, Brotto L, Chittur SV, Breggia A, Stern A, Huang J, Mo C, Seidah NG, et al. (2016). Deletion of Mbtps1 (Pcsk8, S1p, ski-1) gene in osteocytes stimulates soleus muscle regeneration and increased size and contractile force with age. J. Biol. Chem 291, 4308–4322. 10.1074/JBC.M115.686626. [PubMed: 26719336]

25. Chen F, Ni C, Wang X, Cheng R, Pan C, Wang Y, Liang J, Zhang J, Cheng J, Chin YE, et al. (2022). S1P defects cause a new entity of cataract, alopecia, oral mucosal disorder, and psoriasis-like syndrome. EMBO Mol. Med 14, e14904. 10.15252/EMMM.202114904. [PubMed: 35362222]

26. Picard M, Hepple RT, and Burelle Y (2012). Mitochondrial functional specialization in glycolytic and oxidative muscle fibers: tailoring the organelle for optimal function. Am. J. Physiol. Cell Physiol 302, 629–641. 10.1152/AJPCELL.00368.2011.

27. Jornayvaz FR, and Shulman GI (2010). Regulation of mitochondrial biogenesis. Essays Biochem. 47, 69–84. 10.1042/BSE0470069. [PubMed: 20533901]

28. Fujita R, Yoshioka K, Seko D, Suematsu T, Mitsuhashi S, Senoo N, Miura S, Nishino I, and Ono Y Zmynd17 controls muscle mitochondrial quality and whole-body metabolism. FASEB J. 32 5012–5025 10.1096/fj.201701264R.

29. Yoshioka K, Fujita R, Seko D, Suematsu T, Miura S, and Ono Y (2019). Distinct roles of Zmynd17 and PGC1a in mitochondrial quality control and biogenesis in skeletal muscle. Front. Cell Dev. Biol 7, 330. 10.3389/FCELL.2019.00330/BIBTEX. [PubMed: 31921843]

30. Pasut A, Jones AE, and Rudnicki MA (2013). Isolation and culture of individual myofibers and their satellite cells from adult skeletal muscle. J. Vis. Exp, 50074. 10.3791/50074. [PubMed: 23542587]

31. Zhang YE (2017). Non-smad signaling pathways of the TGF-β family. Cold Spring Harb. Perspect. Biol 9, a022129. 10.1101/CSHPERSPECT.A022129. [PubMed: 27864313]

32. Derynck R, and Budi EH (2019). Specificity, versatility and control of TGF-β family signaling. Sci. Signal 12, eaav5183. 10.1126/SCISIGNAL.AAV5183. [PubMed: 30808818]

33. Guillet-Deniau I, Mieulet V, Le Lay S, Achouri Y, Carré D, Girard J, Foufelle F, and Ferré P (2002). Sterol regulatory element binding protein-1c expression and action in rat muscles:

insulin-like effects on the control of glycolytic and lipogenic enzymes and UCP3 gene expression. Diabetes 51, 1722–1728. 10.2337/diabetes.51.6.1722. [PubMed: 12031958]

34. Yang W, Feng B, Meng Y, Wang J, Geng B, Cui Q, Zhang H, Yang Y, and Yang J (2019). FAM3C-YY1 axis is essential for TGFβ-promoted proliferation and migration of human breast cancer MDA-MB-231 cells via the activation of HSF1. J. Cell Mol. Med 23, 3464–3475. 10.1111/JCMM.14243. [PubMed: 30887707]

35. Yan X, Pan J, Xiong W, Cheng M, Sun Y, Zhang S, and Chen Y (2014). Yin Yang 1 (YY1) synergizes with Smad7 to inhibit TGF-β signaling in the nucleus. Sci. China Life Sci 57, 128–136. 10.1007/S11427-013-4581-2. [PubMed: 24369345]

36. Zhang C, Zhu X, Hua Y, Zhao Q, Wang K, Zhen L, Wang G, Lü J,Luo A, Cho WC, et al. (2019). YY1 mediates TGF-β1-induced EMT and pro-fibrogenesis in alveolar epithelial cells. Respir. Res 20, 249. 10.1186/S12931-019-1223-7. [PubMed: 31703732]

37. Kurisaki K, Kurisaki A, Valcourt U, Terentiev AA, Pardali K, Ten Dijke P, Heldin CH, Ericsson J, and Moustakas A (2003). Nuclear factor YY1 inhibits transforming growth factor beta- and bone morphogenetic protein-induced cell differentiation. Mol. Cell Biol 23, 4494–4510. 10.1128/MCB.23.13.4494-4510.2003. [PubMed: 12808092]

38. Schneider CA, Rasband WS, and Eliceiri KW (2012). NIH Image to ImageJ: 25 years of image analysis. Nat. Methods 9, 671–675. 10.1038/NMETH.2089. [PubMed: 22930834]

39. Suzuki Y, Lanner C, Kim J-H, Vilardo PG, Zhang H, Yang J, Cooper LD, Steele M, Kennedy A, Bock CB, et al. (2001). Insulin control of glycogen metabolism in knockout mice lacking the muscle-specific protein phosphatase PP1G/RGL. Mol. Cell Biol 21, 2683–2694. 10.1128/MCB.21.8.2683-2694.2001. [PubMed: 11283248]

40. Guardiola O, Andolfi G, Tirone M, Iavarone F, Brunelli S, and Minchiotti G (2017). Induction of acute skeletal muscle regeneration by cardiotoxin injection. J. Vis. Exp, 54515. 10.3791/54515. [PubMed: 28117768]

41. Biltz NK, Collins KH, Shen KC, Schwartz K, Harris CA, and Meyer GA (2020). Infiltration of intramuscular adipose tissue impairs skeletal muscle contraction. J. Physiol 598, 2669–2683. 10.1113/JP279595. [PubMed: 32358797]

42. Dobin A, Davis CA, Schlesinger F, Drenkow J, Zaleski C, Jha S, Batut P, Chaisson M, and Gingeras TR (2013). STAR: ultrafast universal RNA-seq aligner. Bioinformatics 29, 15–21. 10.1093/BIOINFORMATICS/BTS635. [PubMed: 23104886]

43. Liao Y, Smyth GK, and Shi W (2014). featureCounts: an efficient general purpose program for assigning sequence reads to genomic features. Bioinformatics 30, 923–930. 10.1093/BIOINFORMATICS/BTT656. [PubMed: 24227677]

44. Patro R, Duggal G, Love MI, Irizarry RA, and Kingsford C (2017). Salmon provides fast and bias-aware quantification of transcript expression. Nat. Methods 14, 417–419. 10.1038/NMETH.4197. [PubMed: 28263959]

45. Wang L, Wang S, and Li W (2012). RSeQC: quality control of RNA-seq experiments. Bioinformatics 28, 2184–2185. 10.1093/BIOINFORMATICS/BTS356. [PubMed: 22743226]

46. Robinson MD, McCarthy DJ, and Smyth GK (2010). edgeR: a Bioconductor package for differential expression analysis of digital gene expression data. Bioinformatics 26, 139–140. 10.1093/BIOINFORMATICS/BTP616. [PubMed: 19910308]

47. Ritchie ME, Phipson B, Wu D, Hu Y, Law CW, Shi W, and Smyth GK (2015). Limma powers differential expression analyses for RNA-sequencing and microarray studies. Nucleic Acids Res. 43, e47. 10.1093/NAR/GKV007. [PubMed: 25605792]

48. Liu R, Holik AZ, Su S, Jansz N, Chen K, Leong HS, Blewitt ME, Asselin-Labat ML, Smyth GK, and Ritchie ME (2015). Why weight? Modelling sample and observational level variability improves power in RNA-seq analyses. Nucleic Acids Res. 43, e97. 10.1093/NAR/GKV412. [PubMed: 25925576]

49. Kuznetsov AV, Veksler V, Gellerich FN, Saks V, Margreiter R, and Kunz WS (2008). Analysis of mitochondrial function in situ in permeabilized muscle fibers, tissues and cells. Nat. Protoc 3, 965–976. 10.1038/nprot.2008.61. [PubMed: 18536644]

50. Altman DG, and Bland j.M. (1995). Statistics notes: the normal distribution. BMJ 310, 298. 10.1136/BMJ.310.6975.298. [PubMed: 7866172]

Highlights

- Skeletal-muscle-specific S1P knockout mice have increased muscle mass

- S1P negatively regulates mitochondrial respiration by increasing Mss51 expression
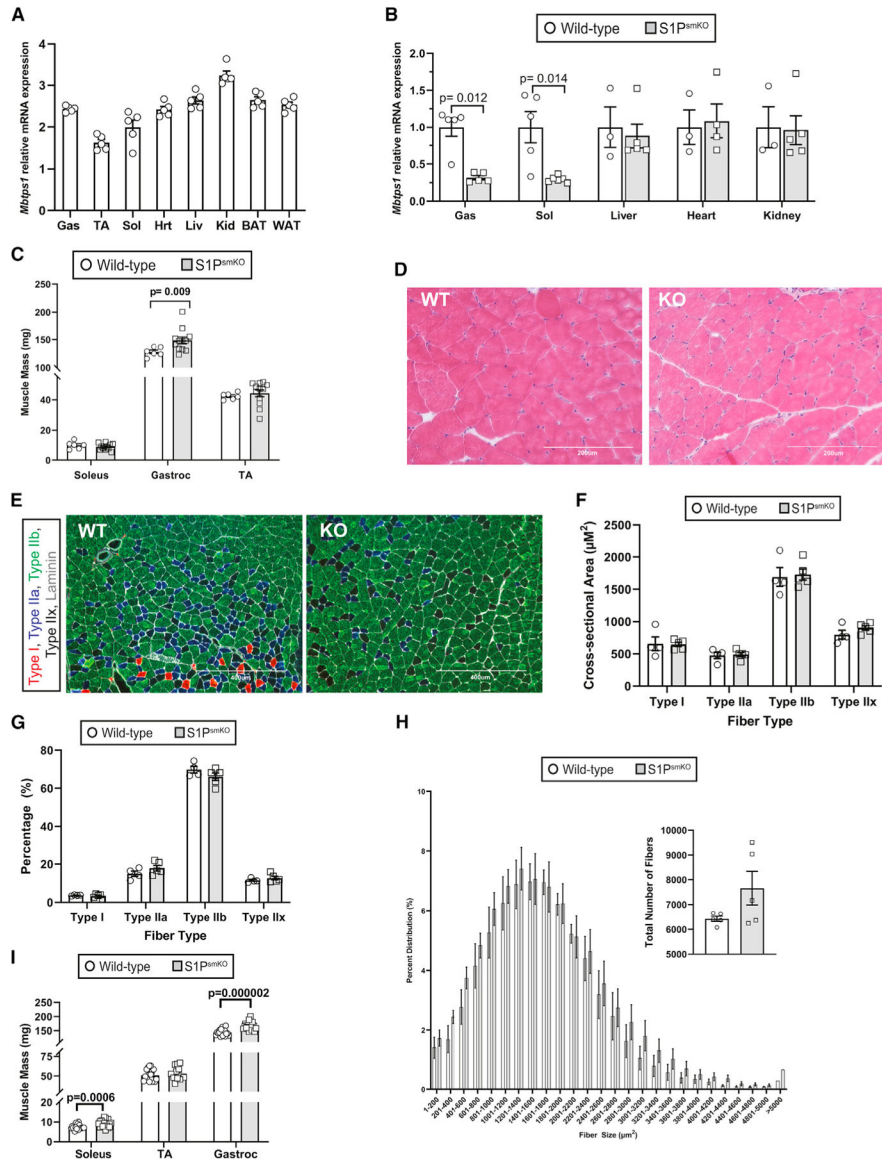
- TGF-β1-driven Mss51 expression is controlled by S1P

Figure 1. S1P depletion in skeletal muscle is associated with increased muscle mass

(A) *Mbtps1* mRNA expression levels in mouse organs.

(B) *Mbtps1* mRNA levels in control (wild type) and S1P^{smKO} skeletal muscles and other organs.

(C) Muscle mass of soleus, gastrocnemius, and TA.

(D and E) H&E and fiber-type staining of the gastrocnemius. Scale bar sizes are indicated.

(F–H) Fiber size (cross-sectional area), percentage distributions of fiber types, total number of fibers, and fiber size distributions. n = 4–5.

(I) Mass of soleus, TA, and gastrocnemius of 97-week-old S1P^{smKO} and wild-type mice. Representative images are shown for (D) and (E). Gas, gastrocnemius; TA, tibialis anterior; Sol, soleus; Hrt, heart; Liv, liver; Kid, kidney; BAT, brown adipose tissue; WAT, white adipose tissue; WT, wild type; KO, knockout. All mice were 12 weeks of age unless noted otherwise. Data are reported as ± SEM. Statistical significance was determined by Wilcoxon

two-sample test and unpaired t test with Satterthwaite adjustment for unequal variances where necessary.
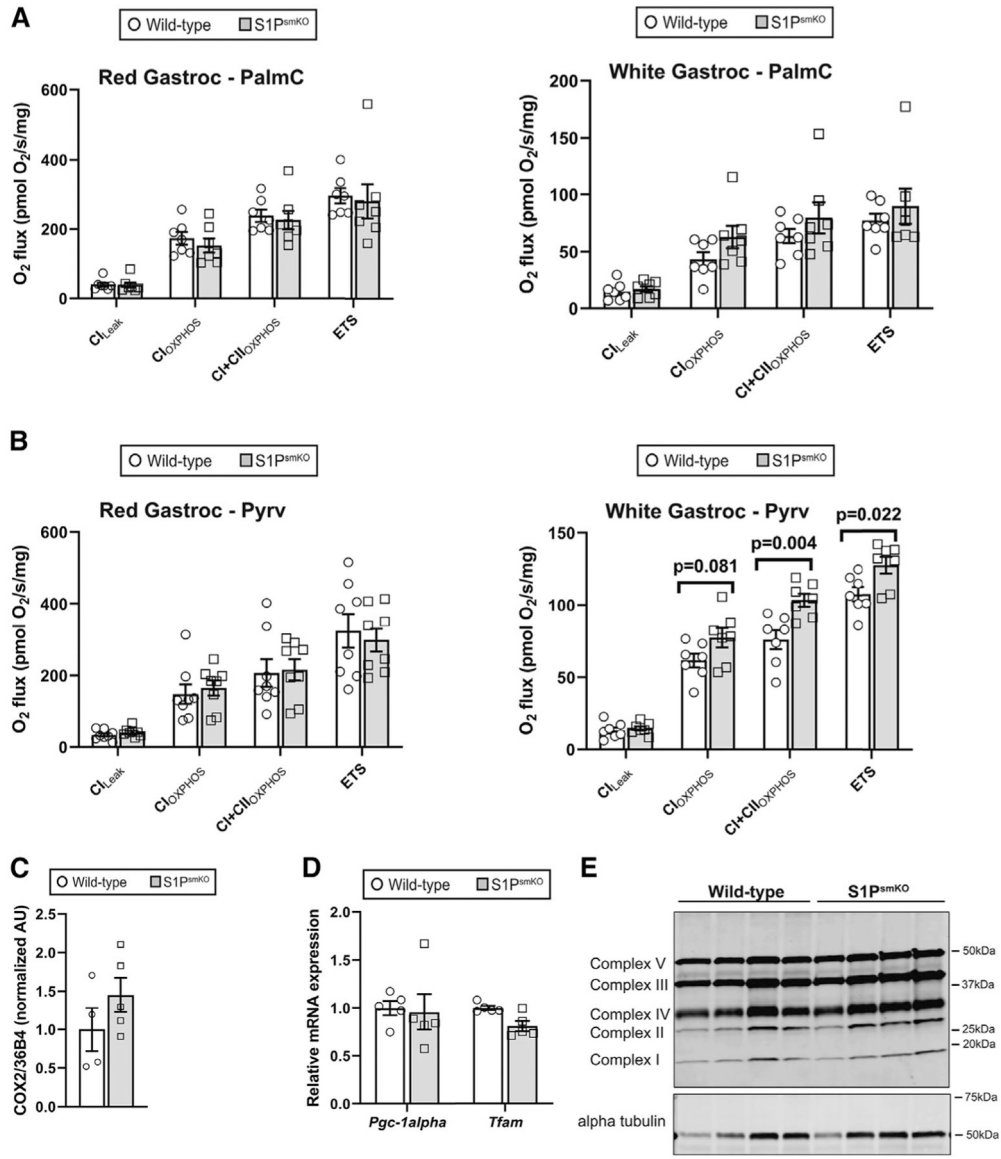
Figure 2. S1P is a negative regulator of mitochondrial respiration

(A and B) Palmitoylcarnitine- (A) and pyruvate-mediated (B) mitochondrial respiration in red and white gastrocnemius.

(C and D) Mitochondrial DNA content and *Pgc-1α* and *Tfam* mRNA levels of the gastrocnemius.

(E) Immunoblotting of oxidative phosphorylation proteins in the gastrocnemius.

PalmC, palmitoylcarnitine; Pyr, pyruvate; ETS, electron transport system. All mice were 12 weeks of age. Data are reported as ± SEM. Statistical significance was determined by unpaired t test and Wilcoxon two-sample test.
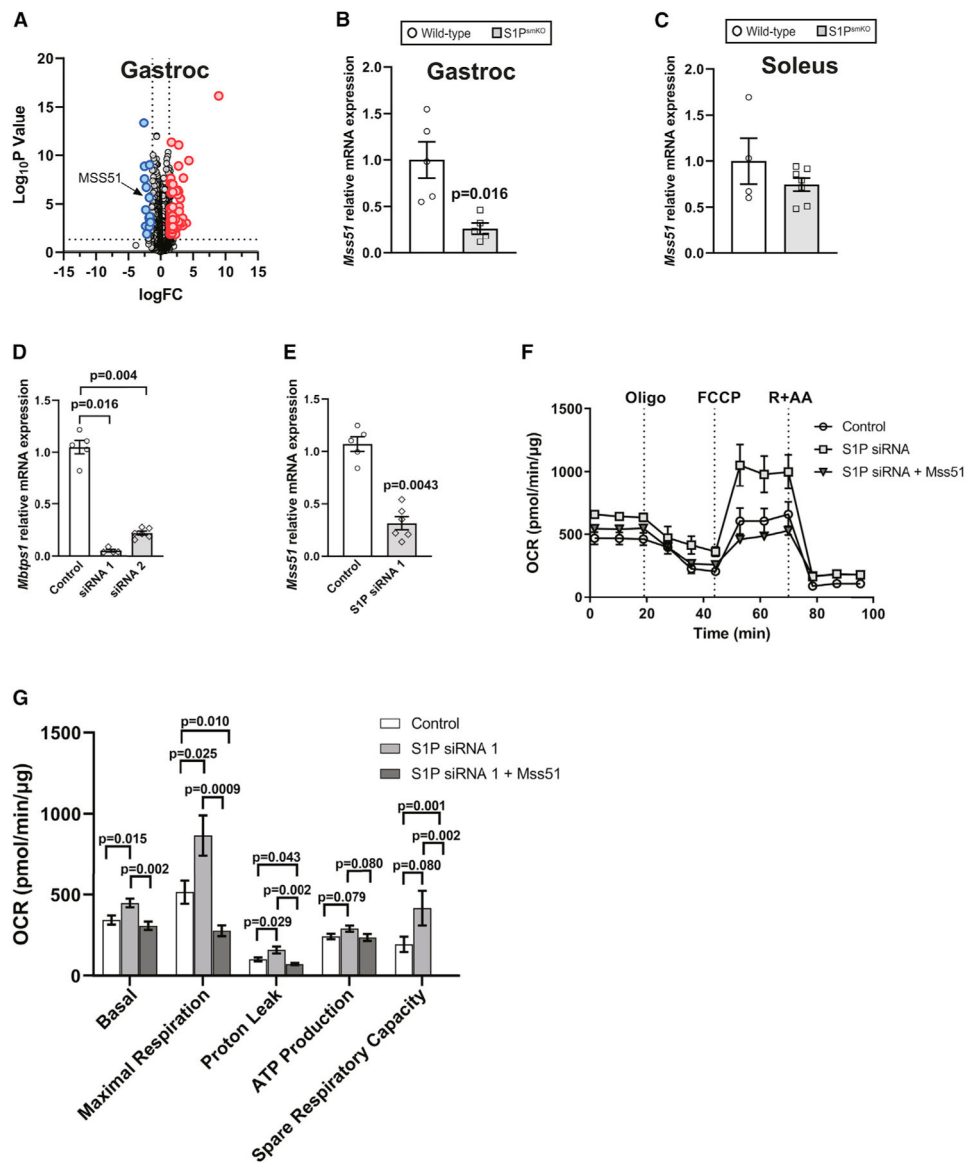
Figure 3. S1P inhibits mitochondrial respiration by promoting Mss51 expression

(A) Volcano plot of genes identified from RNA-seq as significantly differentially increased (red dots) and decreased (blue dots) in gastrocnemius of S1P[smKO] mice relative to wild-type mice. Mss51 is indicated. n = 4 per genotype.

(B) qPCR of *Mss51* mRNA expression in the gastrocnemius.

(C) *Mss51* mRNA expression in the soleus.

(D) Knockdown efficiency of custom *Mbtps1*-targeting siRNAs relative to negative control siRNA in C2C12 cells.

(E) *Mss51* mRNA expression levels in C2C12 cells transfected with control or *Mbtps1*-targeting siRNA (S1P siRNA 1).

(F and G) Oxygen consumption rate of C2C12 cells transfected with control or S1P siRNA 1 plus empty vector or Mss51-FLAG-tagged plasmid (+Mss51) and quantification of respiration parameters. n = 10/group.

OCR, oxygen consumption rate; Oligo, oligomycin; FCCP, carbonyl cyanide p-trifluoro-methoxyphenyl hydrazone; R + AA, rotenone + antimycin A. All mice were 12 weeks of age. Data are reported as ± SEM. Statistical significance was determined by unpaired t test with Satterthwaite adjustment for unequal variances where necessary and Mann-Whitney.
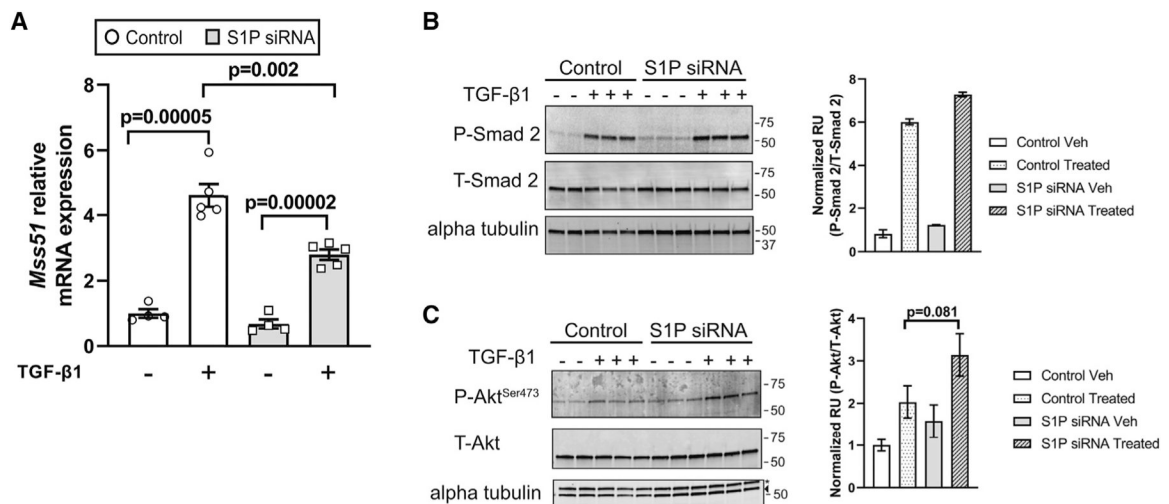
Figure 4. S1P controls Mss51 expression through TGF-β1

(A) *Mss51* mRNA expression levels in negative siRNA (control) and S1P siRNA-transfected C2C12 cells treated with vehicle (−) or TGF-β1 (+).

(B and C) Immunoblots of phosphorylated Smad 2 and total Smad 2 and phosphorylated Akt and total Akt in negative siRNA (control) and S1P siRNA-transfected C2C12 cells treated as in (A) with corresponding densitometry. The arrowhead corresponds to α-tubulin. An asterisk (*) denotes a band corresponding to a different protein since the same blot was probed multiple times to visualize different proteins.

Data are reported as ± SEM. Statistical significance was determined by unpaired t test and Wilcoxon two-sample test.

KEY RESOURCES TABLE

REAGENT or RESOURCE	SOURCE	IDENTIFIER
Antibodies		
OXPHOS (Rodent Antibody cocktail)	Abcam	Cat# MS604–300; RRID: AB_1622581
Phospho-Smad2 (Ser465/467) (Monoclonal, Rabbit)	Cell signaling Technology	Cat# 3108; RRID: AB_490941
Smad 2 (Monoclonal, Rabbit)	Cell signaling Technology	Cat# 5339; RRID: AB_10626777
Alpha tubulin (Monocolonal, mouse)	Sigma Aldrich	Cat# T5168; RRID: AB_477579
Phospho-AKT (Monoclonal, Rabbit)	Cell signaling Technology	Cat# 4060; RRID: AB_2315049
Total-AKT(Monoclonal, mouse)	Cell signaling Technology	Cat# 2920; RRID: AB_1147620
MHC type I	Developmental studies Hybridoma Bank	Cat# BA-F8; RRID: AB_10572253
MHC type IIa	Developmental studies Hybridoma Bank	Cat# SC-71; RRID: AB_2147165
MHC type IIb	Developmental studies Hybridoma Bank	Cat# BF-F3; RRID: AB_2266724
MHC sarcomere	Developmental studies Hybridoma Bank	Cat# MF-20; RRID: AB_2147781
S1P (Polyclonal, Rabbit)	Triple Point Biologics Inc	Cat# 1280
Laminin (Polyclonal, Rabbit)	Abcam	Cat# ab11575; RRID: AB_298179
Chemicals, peptides, and recombinant proteins		
Recombinant Human TGF-β	R&D Systems	Cat# 240-B-002
Critical commercial assays		
DNeasy Blood & Tissue Kit	Qiagen	Cat# 69504
Deposited data		
Gastrocnemius and Soleus S1PsmKO RNA-Seq Data	NCBI GEO	Accession number: GSE199014
Experimental models: Cell lines		
Mouse: C2C12 cells	ATCC	Cat# CRL-1772; RRID: CVCL_0188
Experimental models: Organisms/strains		
Mouse: S1P Floxed C57BL/6J	Yang et al.[22]	N/A
Mouse: B6.Cg-Tg(ACTA1-cre)79Jme/J	Jackson Labs	Cat# 006149; RRID: IMSR_JAX:006149
Mouse: S1P skeletal-muscle-specific knockout Strain	This paper	N/A
Oligonucleotides		
siRNA Negative Control No.1	Life Technologies	Cat# 4390843
Silencer Select Mbtps1 siRNA 2 targeting sequence Sense: CAAUACGUUAAUGUCACCUAtt Antisense: AUGGUGACAUUAACGAUUGtt	Life Technologies	Cat# 430771 siRNA ID: s80604
Silencer Select Mbtps1 siRNA 1 targeting sequence Sense: CAGCUAACAAUGUAAUUAUtt Antisense: AUAAUUACAUUGUUAGCUGtt	Life Technologies	Cat# 4390771 siRNA ID: s80606
Silencer Select Mss51 siRNA targeting sequence Sense: CAUGUUUCCUGAACACCUUtt Antisense: AAGGUGUUCAGGAAACAUGta	Life Technologies	Cat# 4390771 siRNA ID: s93148
Mbtps 1 Primer - See Table S1	This paper	N/A
Cox2 mtDNA Primer - See Table S1	This paper	N/A
36B4 nDNA Primer - See Table S1	This paper	N/A

REAGENT or RESOURCE	SOURCE	IDENTIFIER
36B4 Primer - See Table S1	This paper	N/A
Mss51 Primer - See Table S1	This paper	N/A
Tfam Primer - See Table S1	This paper	N/A
Pgc-1Alpha Primer - See Table S1	This paper	N/A
Acc1 Primer - See Table S1	This paper	N/A
Fasn Primer - See Table S1	This paper	N/A
Col1a1 - See Table S1	This paper	N/A
Col3a1 - See Table S1	This paper	N/A
Fn1 - See Table S1	This paper	N/A
Scd1 Primer - See Table S1	This paper	N/A
Hmgr Primer - See Table S1	This paper	N/A
Ldlr Primer - See Table S1	This paper	N/A
Recombinant DNA		
Plasmid: Mss51-Myc-Flag	Origene	Cat# MR217897
Plasmid: Empty Vector (pCMV6-Entry)	Origene	Cat# PS100001
Plasmid: S1P-Myc-Flag	Origene	Cat# RC212265
Software and algorithms		
SAS software, version 9.4 of the SAS System for Windows	SAS Institute, Inc.	https://www.sas.com/
GraphPad Prism Version 9.0.0	GraphPad Software	https://www.graphpad.com/scientific-software/prism/
ImageJ	Schneider et al.[38]	https://imagej.nih.gov/ij/
LI-COR Image Studio Lite	LI-COR	https://www.licor.com/bio/image-studio-lite/
Seahorse XF Cell Mito Stress Test Report Generator	Wave Software from Agilent	https://www.agilent.com/en/product/cell-analysis/real-time-cell-metabolic-analysis/xf-software/seahorse-wave-desktop-software-740897
DatLab Software 8.0	Oroboros Instruments	https://www.oroboros.at/index.php/product/datlab/

Author Manuscript